Langmuir

ARTICLE

pubs.acs.org/Langmuir

Biofunctionalization of Anisotropic Nanocrystalline Semiconductor−Magnetic Heterostructures

Nicoletta Depalo,[*,†,‡] Pasquale Carrieri,[‡] Roberto Comparelli,[†] Marinella Striccoli,[†] Angela Agostiano,[†,‡] Luca Bertinetti,[§] Claudia Innocenti,[∥] Claudio Sangregorio,[⊥] and M. Lucia Curri[†]

[†]IPCF-CNR, Bari Division, Via Orabona 4, Bari 70126, Italy

[‡]Dipartimento di Chimica, Università di Bari, Via Orabona 4, Bari 70126, Italy

[§]Dipartimento di Chimica, IFM e NIS Center of Excellence, Università Degli Studi di Torino, V. Giuria 7, 10125 Torino, Italy

[∥]Dipartimento di Chimica, Università di Firenze, and INSTM, via della Lastruccia 3, I-50019 Sesto Fiorentino, Italy

[⊥]CNR-ISTM via C. Golgi 19, I-20133 Milano, Italy

Supporting Information

ABSTRACT: Asymmetric binary nanocrystals (BNCs) formed by a spherical γ-Fe_2O_3 magnetic domain epitaxially grown onto a lateral facet of a rodlike anatase TiO_2 nanorod have been functionalized with PEG-terminated phospholipids, resulting in a micellar system that enables the BNC dispersion in aqueous solution. The further processability of the obtained water-soluble BNC including PEG lipid micelles and their use in bioconjugation experiments has been successfully demonstrated by covalently binding to bovine serum albumin (BSA). The whole process has also been preliminarily performed on spherical iron oxide nanocrystals (NCs) and TiO_2 nanorods (NRs), which form single structural units in the heterostructures. Each step has been thoroughly monitored by using optical, structural, and electrophoretic techniques. In addition, an investigation of the magnetic behavior of the iron oxide NCs and BNCs, before and after incorporation into PEG lipid micelles and subsequently bioconjugation, has been carried out, revealing that the magnetic characteristics are mostly retained. The proposed approach to achieving water-soluble anisotropic BNCs and their bioconjugates has a large potential in catalysis and biomedicine and offers key functional building blocks for biosensor applications.

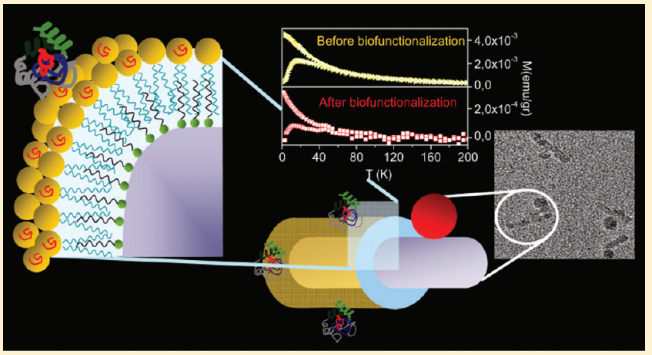

INTRODUCTION

The careful design of a particle surface plays a key role in the creation of tailored nanosized building blocks that can lead to innovative functional materials with a unique potential in fundamental research as well as in a variety of applications. In particular, colloidal chemistry routes can be successfully used to synthesize nanocrystals (NCs) with tunable size from a few up to tens of nanometers, which closely matches the dimensions of a cell (10−100 nm), a protein (5−50 nm), or a gene (2−10 nm), thus indicating such nano-objects as excellent counterparts for interacting with biological targets. The possibility of sharing the same size regime of biomacromolecules, combined with the unique size-dependent properties of NCs, makes them excellent candidates for being successfully employed to obtain hybrid nanobioconjugates and well suited as contrast agents for biomedical imaging, as controlled carriers for drug delivery, and as structural scaffolds for cellular and tissue engineering.[1]

The high-temperature thermolysis of organometallic species in nonpolar solvents has been extensively demonstrated to be a general approach to the synthesis of colloidal NCs over a wide range of compositions, with a narrow size distribution and a high crystalline quality, providing at the same time excellent control of sizes and shapes. Interestingly, recent advances in colloidal synthesis have opened the possibility of producing NCs with very elaborate shapes (i.e., rods, wires, multipods, and stars) having different compositions.[2] In such a wide class of nanoparticles, original and peculiar properties can be achieved because of the coexistence of different functional material domains on the nanoscale.[3] Semiconductor NCs with multiarmed topology, nanorods (NRs) or tetrapods with site-specific deposits of a different materials, and heterostructures made of magnetic, metal, or fluorescent domains are notable examples of complex inorganic architectures that could be ideal candidates for biomedical applications, such as biosensors and contrast agents for the diagnosis of human diseases.[4−6]

As-synthesized NCs are stabilized by an organic molecular layer, thus becoming insoluble in aqueous solution. It is then

Received: November 15, 2010
Revised: April 13, 2011
Published: April 29, 2011

dx.doi.org/10.1021/la200822b | *Langmuir* 2011, 27, 6962–6970

necessary to develop a strategy that is able, through a clever manipulation of the surface chemistry, to achieve a phase transfer of the NCs from the organic to the aqueous phase, providing at same time biostable structures that present suitable anchor points for bioconjugation.

The ideal biocompatible NCs (i.e., objects with a hydrodynamic diameter (D_H) that is smaller than about 100 nm) must be homogeneously dispersed and stable in aqueous solution, exhibit pH and salt stability, show low levels of nonspecific binding to biological components, and maintain their spectroscopic properties.[7] It has proven extremely difficult to achieve each of these features simultaneously.

Several investigations reported the use of PEG (poly(ethylene glycol)) and PEG-based ligands to confer NC water solubility over a wide pH range even at high salt concentrations and to increase the biocompatibility of NC dispersions.[8] PEG is an inert, water-soluble polyether that can be functionalized with a wide range of terminal groups and finds extensive application as a biocompatible coating. Importantly, PEG-functionalized NCs also exhibited reduced nonspecific binding to biological components, reduced cellular toxicity, and increased blood circulation times. Sufficient blood circulation time is critical for biomedical applications, such as imaging and in vivo delivery. Indeed, it also was reported that the in vivo application of surface PEGylation is a powerful strategy for the evasion of the RES (reticuloendothelial system), a defensive mechanism that is able to remove foreign particles or substances from the body, and for protection from nanoparticle degradation.[9]

A successful strategy of NC surface modification exploits hydrophobic interactions between the pristine NC capping layer and PEG-modified phospholipids having different functional terminated groups, which can be used to enable bioconjugation with suitable biological macromolecules.

For example, fluorescent semiconductor NCs (such as core −shell structure CdSe@ZnS, near-infrared-emitting CdTeSe@CdZnS, and cadmium-free $CuInS_2$@ZnS) were encapsulated in a hydrophobic core of PEG phospholipid micelles and used for drug delivery, diagnostic imaging, cancer detection, and sensing.[9c,10] Recently, a simple method of functionalizing the surface of anisotropic gold NRs was also reported with phospholipids.[11] An enhanced stability of phospholipid bilayers in replacing a pristine capping agent (CTAB, cetyltrimethylammonium bromide) was observed in the high-curvature region represented by the rod ends, which were only partially coated with the original stiffer surfactant bilayer of CTAB, thus suggesting an effective role of phospholipids in the surface modification of anisotropic structures.[11]

In this work, the encapsulation of asymmetric binary NCs (BNCs) formed from a semiconductor TiO_2 nanorod joined to a magnetic γ-Fe_2O_3 spherical domain in PEG-modified phospholipids has been performed. The obtained functionalized asymmetric BNCs have been subsequently bioconjugated with bovine serum albumin (BSA), which is a protein of great interest in pharmacology because of its water solubility and biocompatibility, representing a very well studied model system.[12] The functionalization and bioconjugation of the BNCs have been monitored by using optical, structural, and electrophoretic techniques. In addition, the magnetic characteristics of iron oxide NCs (a mixture of both γ-Fe_2O_3 (maghemite) and Fe_3O_4 (magnetite) phases)[13] and BNCs have been evaluated before and after their incorporation into PEG phospholipid micelles and subsequent bioconjugation.

Preliminarly, the functionalization with PEG phospholipids and the subsequent BSA bioconjugation experiment of the iron oxide spherical NCs and TiO_2 NRs, forming the single structural units in heterostructures, have been carried out to obtain a stable micellar system.

The in vivo use of PEG-modified phospholipid micelles containing superparamagnetic iron oxide spherical nanoparticles has been already demonstrated.[8c,14] To the best of our knowledge, this is the first time that PEG-modified phospholipids have been employed to obtain water-soluble TiO_2 NRs and BNCs characterized by anisotropic nanostructures. In addition, the BNCs are very functional hybrid nanostructures possessing a higher level of structural complexity as well as compositional diversity, which enable them to combine the TiO_2 NR photocatalytic activity with the magnetic properties of Fe_2O_3 NCs synergistically.[13]

The overall results show the effectiveness and versatility of the tested PEG lipid system in transferring hydrophobic NCs of different sizes and shapes in aqueous solution, and, even more interestingly, in obtaining stable micellar dispersions under physiological conditions that can be successfully bioconjugated with a suitable protein.

The potential of the obtained water-soluble semiconductor−magnetic heterostructures could have a high impact on catalysis, resulting appealing in microheterogeneous catalytic applications because they combine a highly photoactive material such as anatase TiO_2 NCs with the magnetic properties of Fe_2O_3 NCs.[13,15] The TiO_2 domain could be exploited in catalytic applications whereas the magnetic domain will allow an easy recovery of the catalyst by applying an external magnetic field.[16,17]

The NC surface functionalization by the use of PEG-phospholipids, enabling biocompatibility, can innovatively assist the use of BNCs in biological and in vitro and/or in vivo applications. A large impact can be envisaged in the use of the magnetic domain to drive the biofunctionalized BNCs toward tumor tissues, where magnetically induced hyperthermia can be combined with TiO_2-based photodynamic therapy for cancer treatment.[13]

Indeed, the specific ability of BSA to bind a large variety of ligands makes the BSA/NC conjugates versatile building blocks for suitable organization and order in supramolecular assemblies to fabricate hierarchical nanostructures that are useful in biosensing applications.

EXPERIMENTAL SECTION

Materials. All chemicals were of the highest purity available and were used as received without further purification or distillation. Titanium tetraisopropoxide ($Ti(OPr^i)_4$ or TTIP, 99.999%), trimethylamino-*N*-oxide dihydrate or anhydrous ($(CH_3)_3NO$ or TMAO, 98%), oleic acid ($C_{18}H_{33}CO_2H$ or OLEA, 90), 1-octadecene ($C_{18}H_{36}$ or ODE, 90%), oleyl amine ($C_{17}H_{33}NH_2$ or OLAM, 70%), iron pentacarbonyl ($Fe(CO)_5$, 98%), and dodecan-1,2-diol ($C_{12}H_{24}(OH)_2$ or DDIOL, 90%) were purchased from Aldrich.

Bovine serum albumin (BSA) and reagent-grade salts for the 10 mM phosphate (PBS) and 1 M Tris(hydroxymethyl) aminomethane hydrochloride (Tris-HCl) buffer solutions at pH 7.4 were obtained from Sigma.

1,2-Dipalmitoyl-*sn*-glycero-3-phosphoethanolamine-*N*-[methoxy (poly(ethylene glycol))-2000] (16:0 PEG-2-PE) and, 1,2-distearoyl-*sn*-glycero-3-phosphoethanolamine-*N*-[carboxy(poly(ethylene glycol))-2000]

(DSPE-PEG(2000)carboxylic acid) were purchased from Avanti Polar Lipids.

1-Ethyl-3-(3-dimethylaminopropyl) carbodiimide hydrochloride (EDC) and *N*-hydroxysulfosuccinimide (sulfo-NHS) were purchased from Pierce. Tris-HCl precast gel (4−15% linear gradient) for polyacrylamide electrophoresis, Comassie Brilliant Blue R-250 and a silver stain kit were obtained from BIO-RAD. Bromophenol Blue and glycine were purchased from Sigma-Aldrich.

All solvents used were of analytical grade and purchased from Aldrich. All aqueous solutions were prepared by using water obtained from a Milli-Q gradient A-10 system (Millipore, 18.2 MΩ cm, organic carbon content ≤4 μg/L).

Synthesis of TiO_2 NRs. TiO_2 nanorods were obtained by following literature protocols.[13,18] Briefly, 70 g of oleic acid (OLEA) was dried at 110 °C for 1 h under vigorous stirring and 10 mmol of TTIP was then added, and the resulting solution was reacted with 5 mL of an aqueous 2 M TMAO solution at 100 °C for 96 h. After being cooled, the TiO_2 NRs were separated from their growing mixture upon methanol addition and subsequently subjected to repeated cycles of redispersion and reprecipitation with methanol to wash out surfactant residuals.

Synthesis of Iron Oxide NCs. Spherical iron oxide NCs were synthesized according to procedures reported in the literature.[13,19] A mixture containing ODE (20 mL), DDIOL (2.5 mmol), OLAM (3 mmol), and OLEA (3 mmol) was loaded into a three-necked flask connected to a reflux condenser and dried at 110 °C. It was left stirring for 1 h and then heated under N_2 flux to 250 °C. Subsequently, 1 mL of an $Fe(CO)_5$ solution (1 M) in previously degassed ODE was quickly added to the vigorously stirred mixture. The temperature was then lowered to 130 °C, and the reaction mixture was finally cooled to room temperature after exposure to air for 60 min. Under ambient conditions, a solution containing 2-propanol and acetone (1:1) was added to the mixture, and a black material was precipitated and separated via centrifugation. The black product was dissolved in chloroform to obtain a clear, stable colloidal solution.

Synthesis of BNCs. The BNC synthesis was then carried out exactly according to the procedure used for the iron oxide NCs, as previously reported. The only difference is that a 1 M TiO_2 NR stock solution (0.5 mL) with ODE (20 mL), DDIOL (2.5 mmol), OLAM (3 mmol), and OLEA (3 mmol) was also added to the starting mixture.[13]

Encapsulation of the NCs in PEG-Lipid Micelles. As a general procedure, calibrated amounts of an NC stock solution (500 μL of 1 M TiO_2 NR solution, 300 μL of 1×10^{-2} M iron oxide NC solution, and 300 μL of 1×10^{-2} M of BNC solution) were codissolved in chloroform with 120 μL of 16:0 PEG-2-PE (3.5×10^{-2} M) and 30 μL of DSPE-PEG(2000) carboxylic acid (3.5×10^{-2} M). The employed amount of PEG lipids was about 15 mg.[10b] A dried NC/PEG-lipid layer was attained by chloroform evaporation under N_2 flux and then kept under vacuum for 1 h. The smallest amount of PBS buffer (4 mL at pH 7.4) was added to the film after it was held at 80 °C for 1 min. NC/PEG-lipid micelles were repeatedly heated to 80 °C (with periodic vigorous mixing) and subsequently cooled to room temperature (four cycles). Subsequently larger lipid aggregates were collected as pellets in a centrifuge (13000 rpm for 5 min). The supernatant was recovered and filtered by using 0.2 μm filters (Anotop, Whatman).

Bioconjugation of the NC/Micelles with BSA. The bioconjugation of BSA protein with NC micelles was performed in pH 7.4 PBS buffer at room temperature.[10b,20] A freshly prepared NC/micelle suspension (2 mL) was mixed with freshly prepared EDC and sulfo-NHS solutions, resulting in final concentrations of 0.05 and 5 mM, respectively. BSA protein (2 mg/mL) was added, and the mixture was gently stirred for 90 min. The bioconjugation reaction occurs thanks to EDC, which reacts with carboxyl groups on the NC/micelle surface, forming an amine-reactive *O*-acylisourea intermediate. Sulfo-NHS stabilizes the amine-reactive intermediate by converting it to an amine-reactive sulfo-NHS ester, which is sufficiently stable to react with the native amine groups on the protein, yielding a conjugate of NC micelles and BSA joined by a stable amide bond (Supporting Information, Scheme S1).[20]

The reaction was stopped by the addition of Tris-HCl buffer solution (30 mM). The BSA/NC conjugates were recovered by ultracentrifugation (200 000*g*) and were separated from unreacted cross-linker molecules, quenching agent, and free BSA by repeated cycles of redispersion and reprecipitation with PBS buffer (2 mL).

Photophysical Characterization. Absorption and photoluminescence measurements were performed by means of a UV/vis/NIR Cary 5 spectrophotometer (Varian) and the Eclypse spectrofluorimeter (Varian), respectively. The optical measurements on the NC solution were carried out at room temperature on the solution obtained directly from synthesis without any size-sorting treatments. NC/micelles and BSA/NC conjugates were investigated in PBS buffer at room temperature.

Dynamic Light Scattering. Dynamic light scattering measurements were performed using an LB-550 Horiba particle size analyzer. A 5 mW laser diode (650 nm wavelength) with a fixed detector angle of 177° was used (noninvasive backscattering). The algorithm used to determine the particle size from the light signal includes the Fourier-transformed power spectrum and iterative deconvolution of the relative contribution of variously sized particles in the mixture.

Before measurements were made, freshly prepared samples were filtered using inorganic membrane filter Anotop 10 (0.2 μm, Whatman) to remove any interfering dust particles. DLS measurements were performed at 25 °C.

Transmission Electron Microscopy. Observations of the NCs by high-resolution transmission electron microscopy (HRTEM) were performed with a JEOL 3010-UHR operated at 300 kV. Samples were prepared by dropping a dilute solution of the NCs in toluene on carbon-coated copper grids and then allowing the solvent to evaporate. A statistical analysis was carried out on several low-magnification TEM images. The particle size distributions (PSD) were obtained by counting at least 150 particles for each sample. To measure the length of the TiO_2 NCs in NRs and BNCs, we mostly considered those crystals oriented with the *c* axis of anatase perpendicular to the electron beam; however, a fraction of them could have had a slightly different orientation. The size of the spherical NCs was accurately measurable regardless of the orientation of the iron oxide NCs or the BNCs. Mean particle sizes (d_m) were calculated by using the equation $d_m = \Sigma\, d_i n_i / \Sigma\, n_i$, where n_i is the number of particles of diameter d_i, and the width of the distribution was evaluated by its standard deviation, $\sigma = ((\Sigma\, d_i - d_m)^2 / \Sigma\, n_i)^{0.5}$. High-resolution transmission electron micrographs were filtered using a local 2D Wiener filter (HREM Filters PRO, HREM Research Inc.).

IR Spectroscopy. Midinfrared spectra were acquired with a Perkin-Elmer Spectrum One FTIR spectrometer equipped with a deuterated tryglicine sulfate (DTGS) detector. The spectral resolution used for all experiments was 4 cm^{-1}. For ATR measurements, the internal reflection element (IRE) used was a three-bounce 4-mm-diameter diamond microprism. Cast films have been prepared directly on the internal reflection element by depositing the solution of interest (3−5 μL) onto the upper face of the diamond crystal and allowing the solvent to evaporate.

Gel Electrophoresis. Native PAGE was performed on a 4−15% gradient Tris-HCl precast gel. The gel was characterized after staining with Coomassie Blue and a silver stain kit, respectively.

Magnetic Susceptibility Measurements. The magnetic properties of both powder samples (obtained by gentle evaporation of a $CHCl_3$ solution) and solutions were measured with a cryogenic S600 SQUID magnetometer. The temperature dependence of the magnetization was measured by warming the sample with an applied field of 5 mT after cooling it in a zero field (zero-field-cooled, ZFC, curves) or after

Chart 1. Proposed Mechanism for NC Micelle and BSA/NC Conjugate Formation[a]

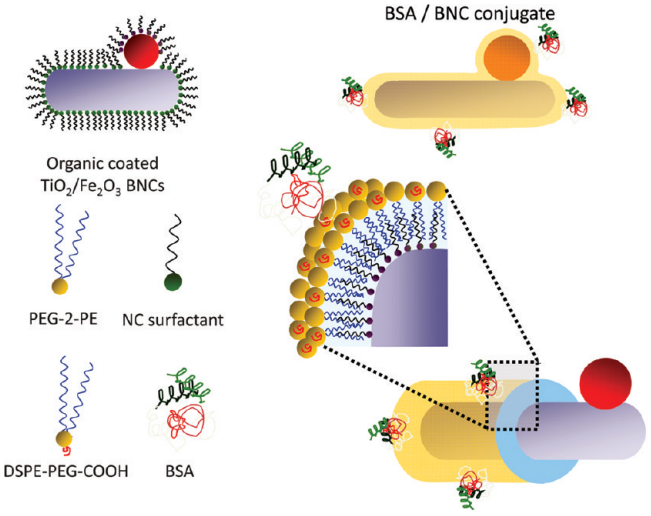

[a]This sketch is merely qualitative. The dimensions of the different components are not to scale.

cooling it in the same probe field (field-cooled, FC, curves). Hysteresis loops were recorded at 2.5 K in the ±5 T range. All data were corrected for the diamagnetism of the sample holder and of the solvent, which were separately measured. ac data on powder samples were collected using an in-house-built susceptometer inserted into a variable-temperature cryostat from Oxford Co. working in the 100−25 000 Hz range.[21]

RESULTS AND DISCUSSION

Organic capped NCs of different shapes and sizes have been successfully embedded in a PEG-modified phospholipid micelle structure, revealing the remarkable versatility of the PEG lipid system in obtaining water-soluble, biocompatible NC/micelle solutions. It is well know that this approach exploits the hydrophobic nature of the NC surface by using PEG-phospholipids whose hydrophobic tails interact with the alkyl chain of the NC capping agent, thus generating micelles that result in a self-assembled monolayer coating the NC. Therefore, PEG portion of the coating confers NC solubility and biocompatibility, but the use of modified PEG enables further functionalization (e.g., by proteins, ligands, or probes).

Subsequently, the NC/PEG lipid micellar complexes have been conjugated with BSA, thanks to the formation of an amide bond between the carboxylic acids group bound to PEG moieties and the primary amine groups of the protein (Chart 1).

Structural and Spectroscopic Characterization of Organic Coated NCs. The as-prepared organic capped NCs have been characterized by DLS and HRTEM measurements. A typical TEM micrograph of the NRs is presented in Figure 1A1. The Figure shows particles with a high aspect ratio (about 10:1), a length in the 10−40 nm range, and a thickness of about 3 to 4 nm, often forming aggregates of several units (up to 10−15). The analysis of the high-resolution images indicates that TiO_2 NRs are anatase single crystals elongated toward the *c* axis (Figure 1A2 and inset). The mean particle length of the NRs, obtained from the PSD (inset in Figure 1A1), is 19 ± 1.6 nm.

The iron oxide NCs exhibit a very homogeneous spherical shape, with a minor fraction of them elongated in a certain direction or with a triangular shape (Figure 1B1). The size of the

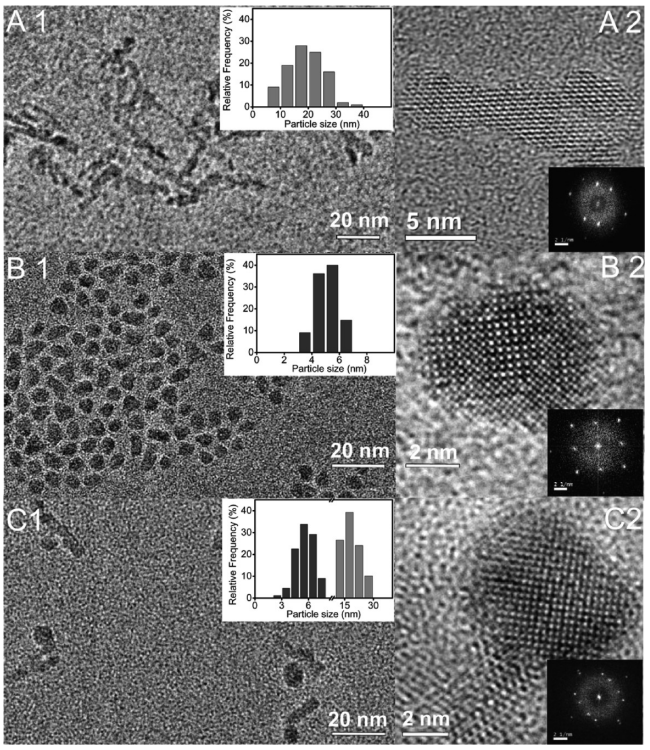

Figure 1. Electron micrograph at low magnification for (A1) TiO_2 NRs, (B1) iron oxide NCs, and (C1) BNCs. (Inset) Particle size distribution of (inset A1) TiO_2 NRs, (inset B1) iron oxide NCs, and (gray) TiO_2 NRs and (black) Fe_2O_3 NCs in (inset C1) BNCs. High-resolution details of (A2) a single TiO_2 NR, (B2) a single iron oxide NC, and (C2) a portion of a single BNC. Fourier transform of (inset A2) a single TiO_2 NR, (inset B2) a single iron oxide NC, and (inset C2) a portion of a single BNC where squares indicate diffraction spots associated with the Fe_2O_3 lattice and triangles indicate diffraction spots associated with the TiO_2 lattice.

particles ranges from 3 to 7 nm with a mean diameter of 5.1 nm and exhibits a narrow distribution (inset in Figure 1B2). As revealed by high-resolution images (Figure 1B2), the observed interference fringe pattern for the iron oxide NCs is compatible with both maghemite and magnetite phases.

Finally, a typical electron micrograph of the BNCs is reported in Figure 1C1. Binary NCs can be easily distinguished, each formed by a rod attached to a sphere. High-resolution images (Figure 1C2) confirmed that the spherical domains and the rods correspond to maghemite or magnetite and anatase, respectively.

In the inset of Figure 1C1, the size distribution of the two phases in BNCs are shown. The iron oxide particles in BNC exhibit a mean particle size of 5.6 nm, which is slightly larger than the value obtained for the iron oxide NCs with a broader distribution (standard deviation of 1.1 nm in BNCs against 0.7 nm in iron oxide NCs). The mean particle length of TiO_2 rods in BNC is 18 ± 1.5 nm, which is about the same as in NRs, but the distribution is narrower.

The results of the TEM investigation of NC size have been compared to those obtained by dynamic light scattering (DLS) measurements. The DLS analysis has been used to monitor the size of particles, the occurrence of possible different size populations in a sample, and the size evolution of the nano-objects along the following steps of functionalization with phospholipids and bioconjugation. To effectively exploit such a powerful analytical

dx.doi.org/10.1021/la200822b |*Langmuir* 2011, 27, 6962–6970

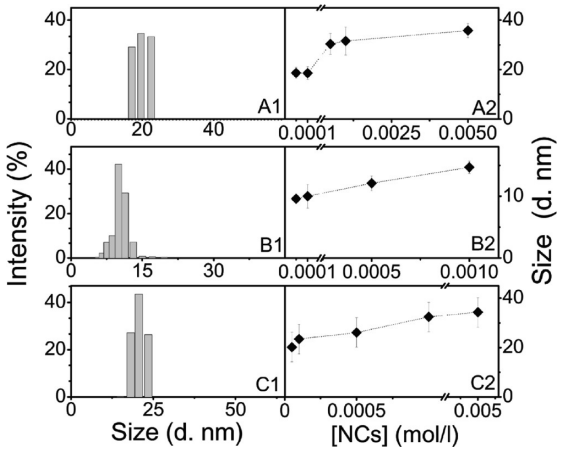

Figure 2. Left panels: Size distribution obtained by DLS of as-synthesized (A1) TiO_2 NRs, (B1) iron oxide NCs, and (C1) BNCs. $[NCs]_{CHCl_3} = 5 \times 10^{-5}$ M for all of the NCs investigated. Right panels: D_H dependence on NC concentration for (A2) TiO_2 NRs, (B2) iron oxide NCs, and (C2) BNCs. All reported data represent mean values and error bars of D_H obtained from five replicates for every tested NC concentration.

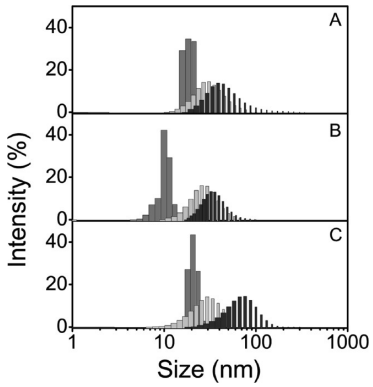

Figure 3. Comparison of D_H distributions of (gray) NCs, (light gray)NC/micelles, and (dark gray) BSA/NC conjugates for (A) TiO_2 NRs, (B) iron oxide NCs, and (C) BNCs.

tool, several parameters influencing the recorded hydrodynamic diameter (D_H) must be taken into account: the particle shape, the nature of the surface-attached ligands, the hydration shells, and the excess counterion binding. For spherical particles, D_H can be obtained by using the Stokes−Einstein equation from the translational diffusion coefficient.[22]

Different types of NCs have been investigated by DLS, namely, as-synthesized hydrophobic NCs suspended in organic solvent: TiO_2 NRs (Figure 2A), iron oxide NCs (Figure 2B), and BNCs (Figure 2C). It is known that a proper dilution should be used to avoid "multiple scattering" phenomena and enhanced particle−particle interaction, such as restricted diffusion, aggregation, and dipolar and magnetic (in the case of iron oxide magnetic particles) interactions, which could all give rise to misleading size values. For this purpose, several measurements have been performed for the different samples for concentration ranging from 5×10^{-3} to 5×10^{-5} M. In the case of iron oxide NCs, at high NC concentration (5×10^{-3} M), DLS experiments failed because the intensity of the scattered light was too high.

In Figure 2A2,B2,C2, the mean values of the average D_H obtained from five replicates for every tested NC concentration are reported. Remarkably, D_H increases at higher NC concentrations, consistent with the assumption of NC aggregate formation that is likely to occur only when NCs are spatially close, as a result of possible hydrophobic interactions among the alkyl chains of capping agents on the NC surface.[23] The overall data indicate that the contribution of NC/NC interactions at the lower limit of the investigated NC concentration range (5×10^{-5} M) can be considered negligible for all of the investigated NC types at the measured size. DLS then provides D_H values that are not affected by particle interactions. In Figure 2A1,B1,C1, the size distributions recorded in the dilute regime (5×10^{-5} M) for TiO_2 NRs, iron oxide NCs, and BNCs, respectively, are reported. In particular for iron oxide NCs, D_H of about 9 ± 2 nm (Figure 2B1) has been found, which is slightly larger than that provided by HRTEM measurements (5 to 6 nm) as usually reported for NCs capped with various hydrophilic coatings.[24] In our case, the difference in size can be accounted for by the presence of the capping agent layer and of a solvent shell.[10b]

In Figure 2A1,C1, DLS measurements performed on TiO_2 NRs and BNCs in the dilute regime are reported, resulting in a monomodal distribution and suggesting that in both cases they are well dispersed in solution without significant aggregation phenomena. The average D_H values obtained are in good agreement with the HRTEM results (a DLS value of 20 ± 1 nm vs an HRTEM value of 18 ± 1.5 nm and a DLS value of 19 ± 2 nm vs an HRTEM value of 19 ± 1.6 nm for BNCs and TiO_2 NRs, respectively).

It is worth noticing that DLS analysis for anisotropic particles, such as TiO_2 NRs and BNCs, have to be cautiously interpreted (Supporting Information) and can be considered to be only qualitative. Nevertheless, such values can be reliable enough to provide a useful indication of the trend in the size evolution of a nano-object along the overall functionalization process.

NCs Containing Phospholipid Micelles and Their Bioconjugation. A DLS investigation of the formation of NC-containing micelles and of the subsequent bioconjugation process has been performed on the as-prepared samples without any further dilution. Indeed, our NC/micelle samples with a PEG lipid concentration of about 3.75 mg/mL are appropriate because they fall in a range where the concentration dependence of the diffusion coefficient for the pure PEG-lipid systems has been shown to be weak (between 1 and 20 mg/mL), thus ultimately excluding intermicellar aggregation phenomena.[25]

The comparison between the D_H values obtained before and after the NC encapsulation in PEG lipids has been reported in Figure 3 and shows a consistent increase in D_H with respect to the hydrophobic NCs values for TiO_2 NRs (Figure 3A), iron oxide NCs (Figure 3B), and BNCs (Figure 3C) along with the occurrence of a monomodal population in all of the investigated samples. First, the increase in D_H values can be reasonably accounted for by the presence of the lipid shell around the NC surface, with possible interdigitation of the hydrophobic tails of the PEG lipid molecules with those of the native capping agents. D_H values recorded for NC/micelles seem to be independent of the initial NC size, also showing a much broader size distribution in all of the investigated NC samples (Table 1).

To account for such evidence, it is worth noting that NC encapsulation in the hydrophobic core of a PEG micelle can occur only starting from high NC concentrations in chloroform (5×10^{-1} M for TiO_2 NRs and 3×10^{-2} M for iron oxide NCs and BNCs). The reported DLS investigation performed on as-synthesized NCs has suggested the occurrence of attractive

Table 1. Hydrodynamic Diameter of As-Prepared NCs and after Incorporation in PEG Lipid Micelles and Bioconjugation[a]

	NC D_H in $CHCl_3$ (nm)	NC/micelle D_H in PBS (nm)	BSA/NC conjugate D_H in PBS (nm)
BNCs	20 ± 1	30 ± 6	68 ± 8
iron oxide NCs	9 ± 2	27 ± 5	43 ± 7
TiO_2 NRs	19 ± 2	30 ± 6	48 ± 8

[a] All reported data represent mean values ± the standard deviation obtained from five replicates.

hydrophobic interparticle interactions that ultimately lead to the formation of NC aggregates in chloroform for NC concentrations higher than 5×10^{-5} M. Therefore, it is reasonable that each micelle may embed not just one NC but aggregates formed by a few NCs, thus resulting in larger micelles once transferred in aqueous solution.

The obtained results are in a good agreement with the recent results reported on spherical luminescent NCs ($CuInS_2/ZnS$) encapsulated in phospholipid micelles, which have been found by TEM and further confirmed by DLS investigation to range from 40 to 90 nm, and encapsulating a variable number of NCs in a single micelle.[9c]

In particular, in the case of the spherical iron oxide NCs the observed larger increase in size (Table 1) can be ascribed to the anisotropy of the NRs and the BNCs, which affects their D_H in chloroform solution and thus has only a limited increase in passing from a single nanoparticle to aggregates in micelles (Supporting Information, Scheme S2).

The bioconjugation reaction with BSA has resulted in a further increase in D_H for all of the investigated samples (Figure 3, Table 1), suggesting covalent binding of the biological molecule to the NC/PEG lipid micelle.

The shift toward high D_H values recorded for BNC bioconjugates was found to be larger than for the TiO_2 NRs and iron oxide NCs counterparts. Such evidence could be due to a larger size and a major structural and geometrical complexity that can introduce an overall size broadening, also considering that more than one BSA molecule can bind a single micelle.

In addition to the bioconjugation procedure, BSA bioconjugate preparation starts from NC micelles characterized by a broad size distribution, which is also reasonable in propagating the products of the bioconjugation reaction, as indeed observed for all of the investigated NCs.

The investigated aqueous micelle suspensions have been found to be stable for several days at 25 °C with no change in the average size and size distribution for all NC types.

It is worth pointing out that the specific adsorption of the protein at the NC micelle surface could be excluded, as demonstrated on a similar system. Indeed, a DLS investigation performed on a reference mixture containing NC micelles and BSA without the linker resulted in two distinct peaks, clearly as a result of the free BSA and the NC micelles.[10b]

The monomodal size distribution of the obtained BSA/NC conjugates stored at room temperature remained unchanged for six days: a slight increase in the D_H value, which is likely explained by the unfolding process of the BSA moiety due to protein aging, was noticed after only 1 week.

Further investigation by FT-IR spectroscopy has been carried out, and the results are shown in Figure 4 for (A) free BSA, (B) BSA/TiO_2 NR conjugates, (C) BSA/iron oxide NC conjugates, and (D) BSA/BNC conjugates. IR signals detected in the investigated samples and their assignments (Table 2) have been compared to the spectra of NC/micelles and to the absorption band frequencies (Supporting Information, Figure S1 and Table S1). The overall data reveal that the peptide backbone structure and the side-chain functional groups have not undergone any significant modification upon BSA conjugation, whereas the shift in C−O−C stretching and the modification of the amide A′ mode suggest the occurrence of a successful bioconjugation reaction evidencing the active participation of C−O−C and the native amine group present in the BSA protein.[10b]

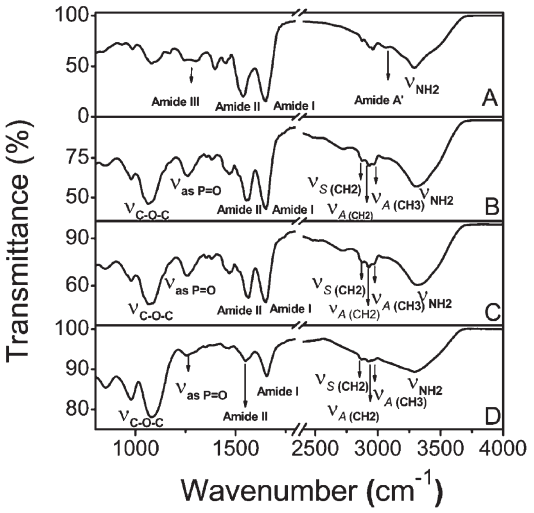

Figure 4. FT-IR-ATR spectra of (A) the pure BSA standard, (B) BSA/TiO_2 NR conjugates, (C) BSA/iron oxide NC conjugates, and (D) BSA/BNC conjugates. All samples were cast from PBS aqueous solution.

Native gel electrophoresis has also been performed to support the occurrence of covalent conjugation between NC micelles and BSA (Supporting Information, Figure S2). After conjugation, the BSA band corresponding to about 66 kDa (free BSA) shifts from 66 kDa to a higher apparent molecular mass in BSA/NC conjugates, suggesting their increase in size with respect to free BSA.

Magnetic Characterization. The magnetic behavior of the iron oxide NCs (A series) embedded in PEG lipid micelles was investigated by measuring the temperature dependence of the magnetic moment after zero-field-cooling (ZFC) and field-cooling (FC) procedures. The obtained results are shown in Figure 5 together with those of the as-synthesized iron oxide NCs that were measured both as a dry powder and dispersed in an organic solvent (chloroform). In all cases, the samples display the typical behavior of single-domain magnetic nanoparticles: at room temperature, all particles are in the superparamagnetic regime, consistent with the small size of the NCs, while below ca. 40 K thermal irreversibility occurs. Accordingly, open hysteresis loops were measured at 2.5 K with a coercivity of a few hundreds of oersteds. The main magnetic parameters obtained from these measurements are listed in Table 3.

The main feature that emerges from the comparison of the data for different samples within the A series is the marked variation of the maxima of the ZFC curves, T_{max}, which as a first approximation corresponds to the average blocking temperature of the system. Moving through the three subsequent steps of

Table 2. IR Signals Detected and Relative Assignments in the Pure BSA Standard and BSA/NC Conjugates

assignment	BSA protein (cm^{-1})	BSA/BNC conjugates (cm^{-1})	BSA/iron oxide NC conjugates (cm^{-1})	BSA/TiO_2 NR conjugates (cm^{-1})
ν_{AS} CH_3	2959	2966	2966	2966
ν	2872	2873	2873	2873
ν_{AS} CH_2	2929	2929	2929	2929
ν	2872	2874	2874	2874
ν_{AS} P═O		1260	1260	1260
ν P−O−C		974	974	974
amide A′	3062			
amide I	1650	1650	1650	1650
amide II	1540	1553	1553	1553
amide III	1302			
amide III	1246			
ν NH_2	3290	3305	3305	3305
ν C−O−C		1061	1061	1061

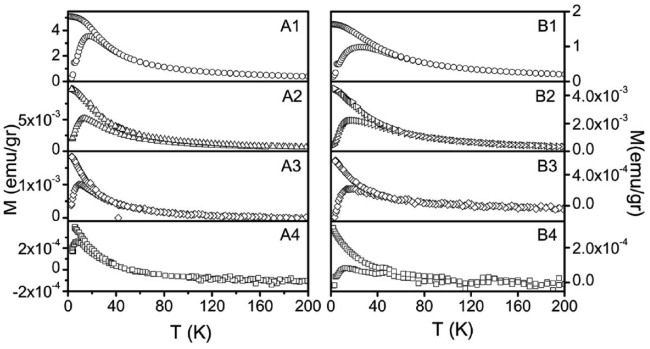

Figure 5. Zfc/Fc curves measured with a 50 Oe magnetic field applied to as-synthesized iron oxide NCs as (A1) a powder, (A2) in organic solvent, (A3) iron oxide NC/micelle aqueous solution, (A4) BSA/iron oxide NC conjugate aqueous solution, (B1) as-synthesized BNCs as a powder, and in (B2) organic solvent, (B3) a BNC/micelle aqueous solution, and (B4) a BSA/BNC conjugate aqueous solution.

the bioconjugate preparation (i.e., from the NC powder to the solution, to iron oxide NC micelles, and to BSA/iron oxide NC conjugates), T_{max} decreases from 18 to 8 K. The low-temperature coercive fields and remnant magnetizations decrease consistently with T_{max}. A similar trend was observed for (B) the BNC series where the observed T_{max} ratio between the powder sample and the BSA/iron oxide conjugate is the same. However, as will be discussed in the following text, the blocking temperatures of the BNCs are always larger than those of the corresponding sample in the NC series.

The first and more relevant mechanism to account for the T_{max} decrease with increasing average distance between the magnetic centers is the progressive lowering influence of dipolar interactions that are known to produce an increase in the average effective energy barrier and a narrowing of their distribution for the particle magnetic moment reversal.[26] However, if dipolar interactions are expected to affect the relaxation dynamics when a dry powder of pristine NCs is considered, it is hard to believe that they can play a relevant role when diluted suspensions of NCs or, even more, iron oxide NC micelles or BSA/iron oxide NC

Table 3. Main Magnetic Parameters of the As-Synthesized Iron Oxide NCs[a]

sample	T_{max} (K)	H_c (Oe)	M_s (emu/g)	M_r/M_s
iron oxide NCs				
A1	18	365	41.2	0.31
A2	14	325		0.28
A3	10	225		0.15
A4	8	260		0.05
BNCs				
B1	27	565	15.9	0.28
B2	18	450		0.21
B3	16	305		0.1
B4	12	285		

[a] As a powder (A1), in an organic solvent (A2), as an iron oxide NC/micelle aqueous solution (A3), as a BSA/iron oxide NC conjugate aqueous solution (A4), as synthesized BNCs as a powder (B1), in an organic solvent (B2), in a BNC/micelle aqueous solution (B3), and in BSA/BNC conjugate aqueous solution (B4) samples. T_{max} = maximum of the ZFC curve; H_C = coercive field; M_S = saturation magnetization; M_r/M_S = remnant magnetization. M_S values were obtained by extrapolating the high-field magnetization values for $1/H \rightarrow 0$.

conjugates are considered. Such a hypothesis is supported by the temperature dependence of the ac susceptibility of the powder samples. In fact, the blocking temperatures obtained from the maxima of the out-of-phase component of the magnetic susceptibility, χ'', for different observation times $\tau = {}^1/_2\pi\nu$, where ν is the frequency of the ac field, could be effectively fitted for both samples to the Arrhenius law (Supporting Information, Figure S3). The best-fit parameters ($\tau_0 \approx 1 \times 10^{-13}$ s) suggest that dipolar fields are not very strong in the powder samples (Supporting Information, Table S2). Therefore, they can be reasonably considered to be negligible upon significant dilution in chloroform. (The particle concentrations are ca. 0.1 and 0.2 w/w for NCs and BNCs, respectively.)

It can be thus inferred that dipolar fields cannot be accounted for as the main parameter responsible for the observed T_{max} behavior, apart from the first step. Alternatively, the encapsulation of iron oxide NCs or BNCs in PEG-modified phospholipids can be assumed to partially affect the magnetic state of surface spins, concurrent with the decreasing in the effective magnetic anisotropy. (For very small particles, such as those investigated in this work, the surface contribution is known to dominate the total magnetic anisotropy.[26])

Because TEM analysis indicates that the average sizes of the magnetic domains in the iron oxide NCs and BNCs are very similar (5.1 ± 0.7 and 5.6 ± 1.1 nm, respectively), it can be instructive to compare their magnetic behavior in order to show the influence of the heterojunction on the maghemite NC properties. For all of the investigated samples, the BNC blocking temperatures are about 50% higher than those of the corresponding iron oxide NCs. The observed difference can be only partially accounted for by the different size: indeed, assuming that $T_{max} \propto KV$, where K is the effective magnetic anisotropy and V is the particle volume, we should expect an increase by a factor of 1.3 only. The interparticle interactions are not responsible for the average energy barrier increase because they are actually expected to be less relevant in the BNCs where the semiconductor rods will keep the magnetic nuclei farther apart from each other. Thus, the result points to a larger magnetic anisotropy

dx.doi.org/10.1021/la200822b |*Langmuir* 2011, 27, 6962–6970

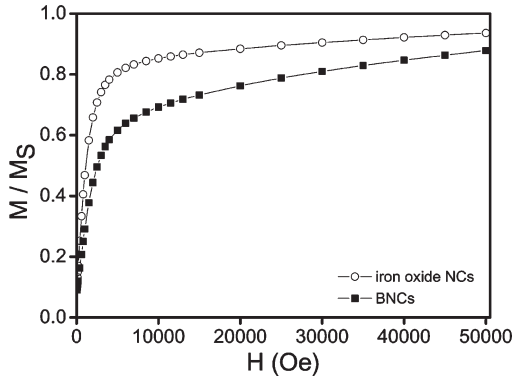

Figure 6. First magnetization curves measured on dry powder at 2.5 K and normalized to the corresponding saturation magnetization values, M_S reported in Table 3.

characterizing the BNCs. This interpretation is corroborated by the larger coercive fields displayed at low temperature by the BNCs samples. The increase in the effective magnetic anisotropy can be ascribed to the breaking of the spin symmetry on the surface occurring at the junction between the Fe_2O_3 and the TiO_2 NRs, which can modify the surface contribution to the total magnetic anisotropy. This interpretation is consistent with recent work reported by Buonsanti et al., who observed a larger anisotropic energy barrier in match-stick Fe_xO_y/TiO_2 nanostructures with respect to physical mixture of Fe_xO_y nanoparticles and TiO_2 nanorods and attributed it to the enhanced shape and surface anisotropy contribution and/or to the modification of local magnetic ordering due to interfacial strain.[27,28]

Finally, it is worthwhile to note that NCs and BNCs exhibit a different approach to saturation, as clearly evidenced by the first magnetization curves normalized to the saturation value extrapolated from the fitting of high-field M vs $1/H$ data. As an example, although NCs are close to saturation at a relatively moderate field (M at 1 T is $0.85M_s$), BNCs require fields larger than 4 T to reach the same percentage of saturation (Figure 6). Such behavior is again consistent with the modification of the spin order at the surface introduced by the presence of an interface with a different metal oxide. It is known, indeed, that a quasi-linear component due to additional surface anisotropy has to be consider when describing the approach to saturation of small particles.[28] In our case, this surface component, which also prevents NCs from saturating in the observed field range, is strongly enhanced by the γ-Fe_2O_3/TiO_2 bounding interface.

CONCLUSIONS

PEG lipid micelles have been used to encapsulate BNCs made of a semiconductor TiO_2 NR joined to a magnetic γ-Fe_2O_3 spherical domain, evidencing the effectiveness of the PEG phospholipids in water solubilizing asymmetric NCs. In addition, a hybrid system has been created by the conjugation of BNC/micelles with BSA. The optical investigation carried out by means of DLS has proven that the obtained BNC/micelles and BSA/BNC conjugates, both with a hydrodynamic diameter smaller than 100 nm, are homogeneously dispersed and sufficiently stable under physiological conditions. In particular, BNC/micelles are stable for about 1 month and BSA/BNC conjugates are stable for 5 to 6 days because of protein aging.

Interestingly, the magnetic features are retained after BNC encapsulation in PEG lipid micelles and the subsequent bioconjugation process, even if decreases in T_{max} and in the effective magnetic anisotropy have been observed in comparison with those of as-synthesized BNCs.

Thanks to the biocompatibility, the overall results suggest that BNC bioconjugates are good candidates for applications in biomedicine. For example, functional PEG-phospholipid-micelle-encapsulated BNCs could be readily conjugated with cancer-specific biomolecules for targeted delivery to the cancerous area, and subsequently magnetically induced hyperthermia, due to the Fe_2O_3 domain in BNCs, could be combined with TiO_2-based photodynamic therapy to kill tumor cells.

In addition, given the exceptional specificity of molecular recognition, the as-prepared BSA/BNC conjugates could be appealing building blocks for creating organized assemblies of nanoparticles on solid substrates that are useful for biosensor fabrication.

ASSOCIATED CONTENT

Supporting Information. Experimental details including FTIR spectra of NC-including micelles, an electrophoresis test, and susceptibility measurements performed on iron oxide NCs and BNCs. This material is available free of charge via the Internet at http://pubs.acs.org.

AUTHOR INFORMATION

Corresponding Author
*E-mail: n.depalo@ba.ipcf.cnr.it.

ACKNOWLEDGMENT

This work has been partially supported by Laboratorio Regionale di Sintesi e Caratterizzazione di Nuovi Materiali Organici e Nanostrutturati per L'Elettronica, Fotonica e Tecnologie Avanzate, n. 20 P.O. PUGLIA 2007-2013, Italy, PRIN 2008, and EC through the NANOTHER project (FP7-NMP4-LA-2008-213631). We gratefully acknowledge Dr. Antonia Mallardi for useful discussions.

REFERENCES

(1) Thanha, N. T. K.; Green, L. A. W. *Nano Today* **2010**, *5*, 213–230.
(2) (a) Kudera, S.; Carbone, L.; Casula, M. F.; Cingolani, R.; Falqui, A.; Snoeck, E.; Parak, W. J.; Manna, L. *Nano Lett.* **2005**, *5*, 445–449. (b) Kamat, P. V. J. *Phys. Chem. B* **2002**, *106*, 7729–7744. (c) El-Sayed, M. A. *Acc. Chem. Res.* **2004**, *37*, 326–333. (d) Lee, S. M.; Cho, S. N.; Cheon, J. *Adv. Mater.* **2003**, *15*, 441–444. (e) Burda, C.; Chen, X.; Narayanan, R.; El-Sayed, M. A. *Chem. Rev.* **2005**, *105*, 1025–1102. (f) Lisiecki, I. J. *Phys. Chem. B* **2005**, *109*, 12231–12244.
(3) (a) Shieh, F.; Saunders, A. E.; Korgel, B. A. *J. Phys. Chem. B* **2005**, *109*, 8538–8542. (b) Gu, H.; Yang, Z.; Gao, J.; Chang, C. K.; Xu, B. *J. Am. Chem. Soc.* **2005**, *127*, 34–35. (c) Yu, H.; Chen, M.; Rice, P. M.; Wang, S. X.; White, R. L.; Sun, S. *Nano Lett.* **2005**, *5*, 379–382. (d) Gao, X.; Yu, L.; Mac-Cuspie, R. I.; Matsui, H. *Adv. Mater.* **2005**, *17*, 426–429.
(4) (a) Bharali, D. J.; Lucey, D. W.; Jayakumar, H.; Pudavar, H. E.; Prasad, P. N. *J. Am. Chem. Soc.* **2005**, *127*, 1364–11371. (b) Levin, C. S.; Bishnoi, S. W.; Grady, N. K.; Halas, N. J. *Anal. Chem.* **2006**, *78*, 277–3281. (c) Gobin, A. M.; Lee, M. H.; Halas, N. J.; James, W. D.; Drezek, R. A.; West, J. L. *Nano Lett.* **2007**, *7*, 929–1934. (d) Huang, X.; El-Sayed, I. H.; Qian, W.; El-Sayed, M. A. *J. Am. Chem. Soc.* **2006**, *128*, 2115–2120.

(5) (a) Fu, A.; Gu, W.; Boussert, B.; Koski, K.; Gerion, D.; Manna, L.; Le Gros, M.; Larabell, C. A.; Alivisatos, A. P. *Nano Lett* **2007**, *7*, 179–182. (b) Yong, K. T.; Qian, J.; Roy, I.; Lee, H. H.; Bergey, E. J.; Tramposch, K. M.; He, S.; Swihart, M. T.; Maitra, A.; Prasad, P. N. *Nano Lett.* **2007**, *7*, 761–765.

(6) (a) Li, C.; Curreli, M.; Lin, H.; Lei, B.; Ishikawa, F. N.; Datar, R.; Cote, R. J.; Thompson, M. E.; Zhoul, C. *J. Am. Chem. Soc.* **2005**, *127*, 12484–12485. (b) Gao, Z.; Agarwal, A.; Trigg, A. D.; Singh, N.; Fang, C.; Tung, C. H.; Fan, Y.; Buddharaju, K. D. *J. Anal. Chem.* **2007**, *79*, 3291–3297.

(7) (a) Laurent, S.; Forge, D.; Port, M.; Roch, A.; Robic, C.; Vander Elst, L.; Muller, R. N. *Chem. Rev.* **2008**, *108*, 2064–2110. (b) Lees, E. E.; Nguyen, T.-L.; Clayton, A. H. A.; Mulvaney, P. *Acs Nano* **2009**, *3*, 1121–1128.

(8) (a) Kievit, F. M.; Veiseh, O.; Bhattarai, N.; Fang, C.; Gunn, J. W.; Lee, D.; Ellenbogen, R. G.; Olson, J. M.; Zhang, M. *Adv. Funct. Mater.* **2009**, *19*, 2244–2251. (b) Yu, W. W.; Chang, E.; Drezek, R.; Colvin, V. L. *Biochem. Biophys. Res. Commun.* **2006**, *348*, 781–786. (c) Fang, C.; Zhang, M. *J. Mater. Chem.* **2009**, *19*, 6258–6266. (d) Kim, D. K.; Dobson, J. *J. Mater. Chem.* **2009**, *19*, 6294–6307. (d) Fan, H. *Chem. Commun.* **2008**, 1383–1394.

(9) (a) Yong, K.-T.; Roy, I.; Swihartab, M. T.; Prasad, P. N. *J. Mater. Chem.* **2009**, *19*, 4655–4672. (b) Liu, W.; Howarth, M.; Greytak, A. B.; Zheng, Y.; Nocera, D. G.; Ting, A. Y.; Bawendi, M. G. *J. Am. Chem. Soc.* **2008**, *130*, 1274–1284. (c) Yong, K.-T.; Roy, I.; Hu, R.; Ding, H.; Cai, H.; Zhu, J.; Zhang, X.; Bergeya, E. J.; Prasada, P. N. *Integr. Biol.* **2010**, *2*, 121–129.

(10) (a) Pons, T.; Lequeux, N.; Mahler, B.; Sasnouski, S.; Fragola, A.; Dubertret, B. *Chem. Mater.* **2009**, *21*, 1418–1424. (b) Depalo, N.; Mallardi, A.; Comparelli, R.; Striccoli, M.; Agostiano, A.; Curri, M. L. *J. Colloid Interface Sci.* **2008**, *325*, 558–566. (c) Dubertret, B.; Skourides, P.; Norris, D. J.; Noireaux, V.; Brivanlou, A. H.; Libchaber, A. *Science* **2002**, *298*, 1795–1762.

(11) Orendorff, C. J.; Alam, T. M.; Sasaki, D. Y.; Bunker, B. C.; Voigt, J. A. *Acs Nano* **2009**, *3*, 971–983.

(12) (a) Housni, A. *J. Phys. Chem. C* **2008**, *112*, 12282–12290. (b) Mikhaylova, M. *Chem. Mater.* **2004**, *16*, 2344–2354.

(13) Buonsanti, R.; Grillo, V.; Carlino, E.; Giannini, C.; Curri, M. L.; Innocenti, C.; Sangregorio, C.; Achterhold, K.; Parak, F. G.; Agostiano, A.; Cozzoli, P. D. *J. Am. Chem. Soc.* **2006**, *128*, 16953–16970.

(14) (a) Thorek, D. L. J.; Chen, A. K.; Czupryna, J.; Tsourkas, A. *Ann. Biomed. Eng.* **2006**, *34*, 23–38. (b) Lu, A. H.; Salabas, E. L.; Schuth, F. *Angew. Chem., Int. Ed.* **2007**, *46*, 1222–1244. (c) Nitin, N.; LaConte, L. E. W.; Zurkiya, O.; Hu, X.; Bao, J. G. *Biol. Inorg. Chem.* **2004**, *9*, 706–712. (d) Mornet, S.; Vasseur, S.; Grasset, F.; Duguet, E. *J. Mater. Chem.* **2004**, *14*, 2161–2175. (e) Yu, W. W.; Chang, E.; Falkner, J. C.; Zhang, J.; Al-Somali, A. M.; Sayes, C. M.; Johns, J.; Drezek, R.; Colvin, V. L. *J. Am. Chem. Soc.* **2007**, *129*, 2871–2879. (f) Qiao, R.; Yang, C.; Gao, M. *J. Mater. Chem.* **2009**, *19*, 6274–6293. (g) Na, H. B.; Hyeon, T. *J. Mater. Chem.* **2009**, *19*, 6267–6273.

(15) (a) Comparelli, R.; Fanizza, E.; Curri, M. L.; Cozzoli, P. D.; Mascolo, G.; Passino, R.; Agostiano, A. *Appl. Catal. B* **2005**, *55*, 81–99. (b) Cozzoli, P. D.; Comparelli, R.; Fanizza, E.; Curri, M. L.; Agostiano, A. *Mater. Sci. Eng. C* **2003**, *23*, 707–713.

(16) Chen, X.; Mao, S. S. *Chem. Rev.* **2007**, *107*, 2891–2959.

(17) Ye, M.; Zhang, Q.; Hu, Y.; Ge, J.; Lu, Z.; He, L.; Chen, Z.; Yin, Y. *Chem.—Eur. J.* **2010**, *16*, 6243–6250.

(18) Cozzoli, P. D.; Kornowski, A.; Weller, H. *J. Am. Chem. Soc.* **2003**, *125*, 14539–14548.

(19) Sun, S.; Zeng, H. *J. Am. Chem. Soc.* **2002**, *124*, 8204–8205.

(20) Wang, S.; Mamedova, N.; Kotov, N. A.; Chen, W.; Studer, J. *Nano Lett.* **2002**, *2*, 817–822.

(21) Midollini, S.; Orlandini, A.; Rosa, P.; Sorace, L. *Inorg. Chem.* **2005**, *44*, 2060–2066.

(22) Zero, K.; Pecora, R. *Dynamic Light Scattering: Applications of Photon Correlation Spectroscopy*; Pecora, R., Ed.; Plenum Press: New York, 1985; p 277.

(23) Fini, P.; Depalo, N.; Comparelli, R.; Curri, M. L.; Striccoli, M.; Castagnolo, M.; Agostiano, A. *J. Therm. Anal. Calorim.* **2008**, *92*, 271–277.

(24) (a) Sperling, R. A.; Liedl, T.; Duhr, S.; Kudera, S.; Zanella, M.; Lin, C. A. J.; Chang, W. H.; Braun, D.; Parak, W. J. *J. Phys. Chem. C* **2007**, *111*, 11552–11559. (b) Pons, T.; Uyeda, H. T.; Medintz, I. L.; Mattoussi, H. *J. Phys. Chem. B* **2006**, *110*, 20308–20316.

(25) Johnsson, M.; Hansson, P.; Edwards, K. *J. Phys. Chem. B* **2001**, *105*, 8420–8430.

(26) Dormann, J. L.; Fiorani, D.; Tronc, E. In *Advances in Chemical Physics*; Prigogine, I., Rice, A., Eds.; Wiley: New York, 1997; Vol. XCVIII, p 283.

(27) Buonsanti, R.; Grillo, V.; Carlino, E.; Giannini, C.; Gozzo, F.; Garcia-Hernandez, M.; Angel Garcia, M.; Cingolani, R.; Cozzoli, P. D. *J. Am. Chem. Soc.* **2010**, *132*, 2437–2464.

(28) (a) Buonsanti, R.; Snoeck, E.; Giannini, C.; Gozzo, F.; Garcia-Hernandez, M.; Garcia, M. A.; Cingolani, R.; Cozzoli, P. D. *Phys. Chem. Chem. Phys.* **2009**, *11*, 3680–3691. (b) Millan, A.; Urtizberea, A.; Silva, N. J. O.; Palacio, F.; Amaral, V. S.; Snoeck, E.; Serin, V. *J. Magn. Magn. Mater.* **2007**, *312*, L5–L9.